

### International Journal of Smart and Nano Materials

ISSN: (Print) (Online) Journal homepage: https://www.tandfonline.com/loi/tsnm20

# Interplay between entanglement and crosslinking in determining mechanical behaviors of polymer networks

Yuhao Liu, Weikang Xian, Jinlong He & Ying Li

**To cite this article:** Yuhao Liu, Weikang Xian, Jinlong He & Ying Li (2023) Interplay between entanglement and crosslinking in determining mechanical behaviors of polymer networks, International Journal of Smart and Nano Materials, 14:4, 474-495, DOI: 10.1080/19475411.2023.2261777

To link to this article: <a href="https://doi.org/10.1080/19475411.2023.2261777">https://doi.org/10.1080/19475411.2023.2261777</a>

9	© 2023 The Author(s). Published by Inform UK Limited, trading as Taylor & Francis Group.
<b>+</b>	View supplementary material 🗗
	Published online: 28 Nov 2023.
	Submit your article to this journal 🗷
ılıl	Article views: 828
a`	View related articles 🗹
CrossMark	View Crossmark data ☑







## Interplay between entanglement and crosslinking in determining mechanical behaviors of polymer networks

Yuhao Liu\*, Weikang Xian\*, Jinlong He\* and Ying Li\*

Department of Mechanical Engineering, University of Wisconsin-Madison, Madison, WI, USA

#### **ABSTRACT**

In polymer physics, the concept of entanglement refers to the topological constraints between long polymer chains that are closely packed together. Both theory and experimentation suggest that entanglement has a significant influence on the mechanical properties of polymers. This indicates its promise for materials design across various applications. However, understanding the relationship between entanglement and mechanical properties is complex, especially due to challenges related to length scale constraints and the difficulties of direct experimental observation. This research delves into how the polymer network structure changes when deformed. We specifically examine the relationship between entanglement, crosslinked networks, and their roles in stretching both entangled and unentangled polymer systems. For unentangled polymers, our findings underscore the pivotal role of crosslinking bond strength in determining the system's overall strength and resistance to deformation. As for entangled polymers, entanglement plays a pivotal role in load bearing during the initial stretching stage, preserving the integrity of the polymer network. As the stretching continues and entanglement diminishes, the responsibility for bearing the load increasingly shifts to the crosslinking network, signifying a critical change in the system's behavior. We noted a linear correlation between the increase in entanglement and the rise in tensile stress during the initial stretching stage. Conversely, the destruction of the network correlates with a decrease in tensile stress in the later stage. The findings provide vital insights into the complex dynamics between entanglement and crosslinking in the stretching processes of polymer networks, offering valuable guidance for future manipulation and design of polymer materials to achieve desired mechanical properties.

#### **ARTICLE HISTORY**

Received 17 July 2023 Accepted 18 September 2023

#### **KEYWORDS**

Entanglement; crosslinking networks; mechanical property; microstructure evolution; molecular dynamics simulation

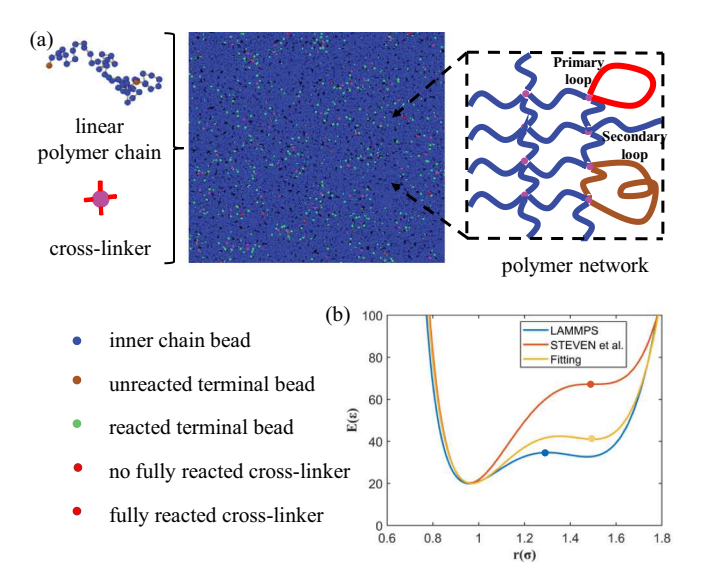
CONTACT Ying Li yli2562@wisc.edu Department of Mechanical Engineering, University of Wisconsin-Madison, Madison, WI 53706, USA

\*These authors contributed equally to this work.

Supplemental data for this article can be accessed online at https://doi.org/10.1080/19475411.2023.2261777

© 2023 The Author(s). Published by Informa UK Limited, trading as Taylor & Francis Group.

This is an Open Access article distributed under the terms of the Creative Commons Attribution-NonCommercial License (http://creativecommons.org/licenses/by-nc/4.0/), which permits unrestricted non-commercial use, distribution, and reproduction in any medium, provided the original work is properly cited. The terms on which this article has been published allow the posting of the Accepted Manuscript in a repository by the author(s) or with their consent.



#### 1. Introduction

Entanglement, in polymer physics, is defined as the topological constraint between sufficiently long polymer chains when they are close to each other. Discussions of the entanglement date back to 1940 in Treloar's study of rubber elasticity [1]. The effects of the entanglement have been successfully conceptualized by the tube model that depicts the overall restriction from the bulk polymer on a single chain as a tube-like region [2]. Many models have been proposed [3–9] and the essence of these models is the quantification of the strength of the entanglement and how the entanglement affects the elasticity of the polymer network, under different magnitudes of deformation. In addition, entanglement is equivalently important in understanding the dynamics of amorphous linear, branched, and star polymers. The concept of reptation was initially introduced by de Gennes [10] and then further developed by Edwards and Doi [11]. The reptation model quantifies the one-dimensional thermal motion of a linear chain with molecular weight M in the tube-like region and predicts the relaxation time tau ~ M³, which is close to the relation of tau ~ M³.4 based on experimental observations [12]. It is worth noting that, the description mentioned above is applicable for polymer melt, not the solution.

While many constitutive models primarily address networks in their dry state, exploring the relationship between the mechanical properties of entangled networks and their various final preparation conditions is fascinating. A recent theoretical study revealed that versatile states of entanglement, and thus different mechanical properties of the networks, can be achieved by alternating the concentration of polymer in preparation and final conditions [13]. On the other hand, experimental studies have also demonstrated the interplay between the entanglement and the mechanical properties of the polymer networks. For example, vinyl-terminated polydimethylsiloxane (PDMS) crosslinked in solutions at low concentrations showed significant enhancement of the maximum stretch upon which the PDMS networks broke compared with those crosslinked in the bulk state [14]. However, recent studies have demonstrated that hydrogels prepared in higher concentrations and thus more entangled states present improvement in both the modulus and the

toughness, compared with regular hydrogels that are usually prepared in dilute solution [15]. The nontrivial entanglement-mechanical properties correlation offers the possibility of developing new materials in a wide range of applications. Peptide-crosslinked hydrogels in highly entangled states can achieve even higher fracture toughness and fatigue resistance [16]. Protein-based hydrogels that harness the advantage of entanglement are promising candidates for biocompatible implants [17]. The entanglement with other reinforcement mechanisms can produce synergetic effects that further improve the mechanical properties of the networks or their composites. For instance, microspheres grafted with poly(acrylic acid) chains in gel state show improved strength because the acrylic acid chains can form an abundant amount of hydrogen bonds [18]. Inspired by the composite-like nature of cartilage, Soltanahmadi et al. grafted polyacrylamide into PDMS sponge and the gelelastomer composite demonstrates load-bearing capabilities with improved energy dissipations while maintaining its stiffness. Interestingly, the advantageous features of microscopic entanglement can also be transferred to larger scales. Micro hydrogel strands fabricated by pressing bulk hydrogel through a sieve with micrometer pores tangled and intertwined to form stable gel-like materials, which not only demonstrated desirable mechanical properties but also led to rapid tissue maturation [19]. Fracture is an important failure mode in many applications. Efforts to understand the fracture properties of polymeric networks has been devoted for over a half of century after Lake and Thomas proposed the classic fracture model [20], although questions remain, especially with entangled networks. For example, the fracture toughness of entangled network is much higher than the intrinsic toughness predicted by the Lake-Thomas model, with the improvement attributed to the dissipative effect of the entanglement near the crack-tip [21]. The dissipation due to the entanglement can be captured theoretical models that consider the interplay between chain scission and entanglement evolution at different length scales [22] and in different directions [23]. Adopting microscopic models that describe the scission of the chains in the networks is necessary in developing the macroscopic models. But such microscopic models are also challenging to establish. For example, Lamont et al. described the micromechanics of slide-ring networks, that are similar the entangled networks, by using an extendable Langevin chain model [24]. But such a singlechain model may misinterpret the effect of the entanglement, which is essentially multichain interaction. In addition, the connection between the micro- and the mesoscopic structural evolution may become difficult to trace when one tries to integrate them and to establish multiscale models [25] because the macroscopic fractures of the networks are hierarchical processes, which involve different zones near the crack-tip [26].

It is also challenging to quantify the entanglement-mechanical properties correlation because the entanglement is intrinsically constrained at a length scale of about tens of nanometer (orders of tube diameter  $a_{pp}$ ). Therefore, direct characterization of the entangled chains at atomistic or nanometer scales by experimental techniques is also nontrivial. Single-molecule fluorescence microscopy is used to closely observe tube-like constraints [27]. On the other hand, methods like rheological measurements [28], scattering-based techniques [29], and dielectric spectroscopy [30] are used more frequently. Molecular simulation is another important approach to study the entanglement-mechanical properties correlation because it can not only determine clearly the structures of the entanglement [31] but also track the corresponding evolution [32]. The tube-like region can be identified by

averaging time-dependent trajectories of the polymer chains [33], by minimizing the configurations of the chains with the uncrossability between different chains enforced [34], or by the geometric method that does not rely on energy minimization [35,36]. With the structure and dynamics explicitly specified, the connection between the entanglement and the mechanical properties can be studied rigorously. For example, the viscoelasticity of melts of linear polymer can be quantitatively predicted with the aid of molecular dynamics (MD) simulations [32,37]. MD simulations have been also used to establish the entanglement-mechanical properties relation. In the MD simulations by Silozberg et al. [38], it is shown that the entanglements trapped between crosslinks contribute the most to the fracture energy as the contribution from the crosslinks is very limited since the density of the crosslinks is low, which is recently further confirmed experimentally [15]. In addition, Umeno et al. studied the fracture process in polycarbonate via coarsegrained molecular dynamics (CGMD) simulations and found that the brittle-ductile failure mode transition is related to the molecular weight of change from unentangled to entangled regime [39]. In the more complicated double network systems, the synergetic of the short and the long chains can be also elucidated by MD simulations. Higuchi et al. showed that the short components increase the elasticity, while the long chains improve the ductility [40]. However, the spatial scales in the simulations of these works are limited, such as the structure of the entanglements; thus, its relation to the mechanical properties of the networks is not fully elucidated. In this study, we offer a detailed analysis of the structural evolution of the unentangled and entangled networks under tensile deformation until complete fracture, by using MD simulations with up to over 4 million beads in the systems. The evolutions of microstructures are tracked to shed light on the mechanical responses of these polymer networks.

In this study, we explore the structural evolution of deformed polymer networks through molecular dynamics (MD) simulations, emphasizing the important role played by entanglements between polymer chains. Our research elucidates the role of the crosslinking network in unentangled polymer systems and the combined roles of entanglement and crosslinking networks in entangled polymer systems, aiming to guide the future design of polymers with advanced mechanical properties, such as high strength and fatigue tolerance.

#### 2. Methods

In this section, we introduce the computational model used in this work and the simulation protocol. Equilibrated melts were first generated and then endcrosslinked to form networks. A snapshot of one of the networks is shown in Figure 1(a). Trajectories from MD simulations were used to quantify the mechanical responses and the structure of the polymer networks. The Z1+ algorithm [36] was used to process the trajectories of the polymer networks to extract information on the entanglement. In this paper, all quantities are in reduced LJ units.

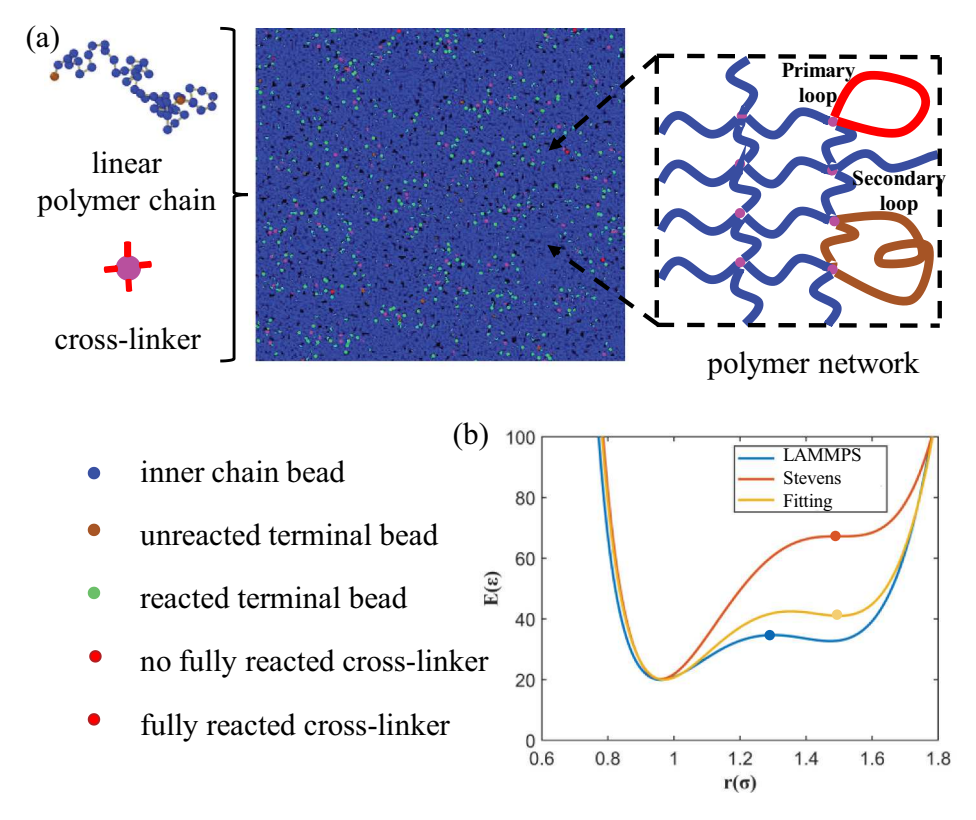


**Figure 1.** Simulation models of polymer networks: (a) the configuration of built polymer network is formed by end-crosslinking the linear polymer chains and cross-linkers. The zoom-in figure is a snapshot showing the network, and (b) three groups of quartic parameters values used in this paper.

#### 2.1. FENE model

The finite extensible nonlinear elastic (FENE) model is essentially generic and coarse-grained and has been widely used to understand structural and dynamic properties of different polymeric systems like linear and branched polymer melts, polymer solutions, and networks. The potential setting for the FENE model includes Weeks-Chandler-Anderson (WCA) potential and FENE potential. The WCA potential, given by Eq. 1, is applied to all the possible pairs of beads in the system. The WCA potential is purely repulsive within the range of the assigned cutoff distance.

$$U_{\text{WCA}}(r) = \begin{cases} 4\varepsilon \left[ \left(\frac{\sigma_{i}}{r}\right)^{12} - \left(\frac{\sigma_{i}}{r}\right)^{6} + \frac{1}{4} \right], r < 2^{1/6}\sigma \\ 0, r \ge 2^{1/6}\sigma \end{cases}$$
 (1)

In this model, a polymer chain is simplified as a string of beads that are connected by a nonlinear spring [41], represented by the FENE potential as given in Eq. 2, where k = 30 and R = 1.5 are standard choices. The separation distance between two beads is r. The energy and length units  $\varepsilon$  and  $\sigma$ , together with the mass of bead  $m_b$ , set the time unit as  $\tau = \sigma_L \sqrt{m_b/\varepsilon}$ .



$$U_{\text{FENE}}(r) = -\frac{kR^2}{2} \ln\left(1 - \frac{r^2}{R^2}\right) \tag{2}$$

This standard choice of parameters results in the average bond length  $l_b = 0.965$  when the  $k_BT$  is equal to  $\in$ . Although the addition of a bending interaction between two consecutive bonds [42] enables correlating the FENE model to specific polymers, we did not include the angle potential since such angle potential is in contradiction to the implementation of the quartic potential defined later. The number density was chosen as the standard value for the FENE model from the reference [41]. The choice of the number density ensures that around 3 beads effectively represent a Kuhn segment. More importantly, the choice, together with other model parameters, ensures the correct entanglement strands per entanglement volume. In addition, the dynamics of system is evolved according to the Langevin equation (Eg. 3):

$$m_b \frac{\partial \mathbf{R}_n}{\partial t^2} = -\nabla U - \Gamma \frac{\partial \mathbf{R}_n}{\partial t} + \xi \tag{3}$$

where updates of the positions of the beads,  $R_n$ , are based on the total of the given potentials  $U = U_{WCA} + U_{FENE}$ , the friction  $\Gamma = 0.5$ , and the stochastic force  $\xi$  that has statistics  $\langle \xi \rangle = 0$  and  $\xi_n(t)\xi_m(t') = 6\varepsilon\Gamma/\Delta t\delta_{nm}\delta(t-t')\mathbf{I}$ .  $\Delta t$  is the timestep set as 0.01.  $\delta$ is the kronecker delta function. I is the unit tensor. The Velocity-Verlet time integration scheme is used to integrate the Langevin equation. All simulations were conducted in LAMMPS package [43]. NVE ensemble was used in generation and equilibration of the network, while NVT ensemble was used in the uniaxial tensile process. The temperature was set 1.0 in all NVT ensembles.

#### 2.2. Simulation protocol

Systems with different chain lengths were built with the parameters detailed in Table 1 and the flowchart shown in Figure S1. In the first step, corresponding precursor melts were generated and equilibrated. Generation of the pre-

Table 1. Simulated cross-linked polymer networks. N is the polymerization degree of the chain between two adjacent cross-linkers;  $n_{\rm ch}$  and  $n_{\rm ck}$  denote the number of polymer chains and crosslinkers, respectively, L is the simulation box side length, and  $\langle \phi 
angle$  is the cross-linking functionality of the cross-linker.  $\langle R_{ee}^2 \rangle^{1/2}$  is the measured mean end-to-end distance of cross-linked chains.  $L_{pp0}$  and  $a_{pp0}$  are the mean contour length of the primitive chain and tube diameter, respectively.  $\langle z_{kink} \rangle$  and  $\langle z_{\text{coil}} \rangle$  characterize the number of entanglements per chain defined by the kink and coil assumptions, respectively.

N	n <sub>ch</sub>	n <sub>ck</sub>	L	<φ>	$\left\langle R_{ee}^2 \right\rangle^{1/2}$	$L_{pp0}$	$a_{pp0}$	< z <sub>kink</sub> >	< z <sub>coil</sub> >
20	5000	2500	49.0	3.91	5.53	5.035	5.443	0. 197	0.107
30	3000	1500	47.3	3.91	6.52	5.971	6.211	0.532	0.292
50	2000	1000	49.0	3.89	9.10	1.191	8.621	0.874	0.468
100	400	200	36.1	3.80	13.08	17.830	9.587	2.230	1.351
200	600	300	52.1	3.85	19.50	31.610	1.511	4.568	2.483
300	600	300	59.6	3.87	23.35	45.691	11.064	7.535	3.834
800	500	250	77.8	3.81	37.85	107.430	11.738	15.832	8.652
1000	600	300	89.1	3.82	41.30	135.470	11.952	20.328	10.970
4204	1034	517	172.3	3.79	87.651	631.547	12.165	113.154	50.164
8408	517	259	172.3	3.82	124.334	1254.520	12.323	227.739	100.076

equilibrated melts was achieved by placing random-walk chains in the simulation box with periodic boundary conditions in all three directions that were remained in all following simulations. A soft pairwise interaction was used to push overlapped beads off from each other to ensure the numerical stability of the following simulations with WCA potential [44].

In the second step, the pushed-off configurations were relaxed, in a hybrid MD/MC way, using the bond swap algorithm [45]. It is worth noting that only the unentangled and slightly entangled were obtained by the described methods (N20-N1000). N is the polymerization degree of the chain between two adjacent cross-linkers. The equilibrated configurations for the highly entangled systems (N4204 and N8408) were obtained from work by Svaneborg and Everaers [46]. In the third step, networks were formed using a method that emulated end-crosslinking that maintains the chain lengths between crosslinkers. This means the crosslinking reaction could only occur at the chain-ends. While a free radical-like reaction is more effective at forming these networks, this approach results in a logarithmic distribution of chain lengths [47,48]. Stoichiometric amount of crosslinker beads with functionality  $\phi_{max} = 4$  was added in the simulation boxes randomly, followed by short push-off runs to avoid overlap between beads and by relaxation runs to ensure the crosslinker are well-dispersed. The densities of the systems slightly changed after the inclusion of crosslinkers. But no change in the dimensions of the simulation boxes was applied to compensate for the densities. The crosslinking reactions were simulated according to a geometric criterion ( $R_{cut} = 1.5$ ) and an assigned probability p = 0.5. A crosslinker is deactivated once it reacts with four chain ends and its crosslinking reaction can no longer happen. For the N50 systems, reactions that last  $3.5 \times 10^8$  timesteps were sufficient to complete the crosslinking process with the functionalities over 3.8, as shown in Figure S2. For the systems with longer chains, another method was used to extend the crosslinking reaction because the successful rate of creating bonds drops significantly with longer chain and thus lower number density of the chain ends [47]. In Figure S2, the rate of bond creation drops significantly with the progression of the reaction because the number of available reactants decreases. Averaged number of bonds per crosslinker increased from 0 to 3.5 in about  $0.5 \times 10^6$ while it took  $3.0 \times 10^6$  to increase the number from 3.5 to 3.8.

The extension consists of four steps, as shown in Figure 2. As the reaction progressed, unsaturated crosslinkers emerged as potential candidates for further reactions. For each candidate, a search was conducted for available chain ends within a broader geometric range to identify possible partners ( $R_{\rm cut}=0.1L$ ). A certain number of partners with the shortest separation distances were picked according to the candidate's availability. Harmonic bonds with soft potential are then created between the candidates and their partners. Then, relaxations were performed with the soft harmonic potential applied to the paired crosslinkers and chain ends to decrease the lengths of the harmonic bonds close to the equilibrium bond length of the FENE bond. Finally, the harmonic potential was then replaced by the FENE potential, followed by a short relaxation in FENE and WCA potential. The mean-squared internal distances (MSID) of the networks after the extended reaction is shown in Figure S3, which that the method does not alter the structure of the linear chain significantly. Finally, the FENE potential was replaced by the quartic potential, given in Equation 4, to simulate the bond breaking during the deformation process.

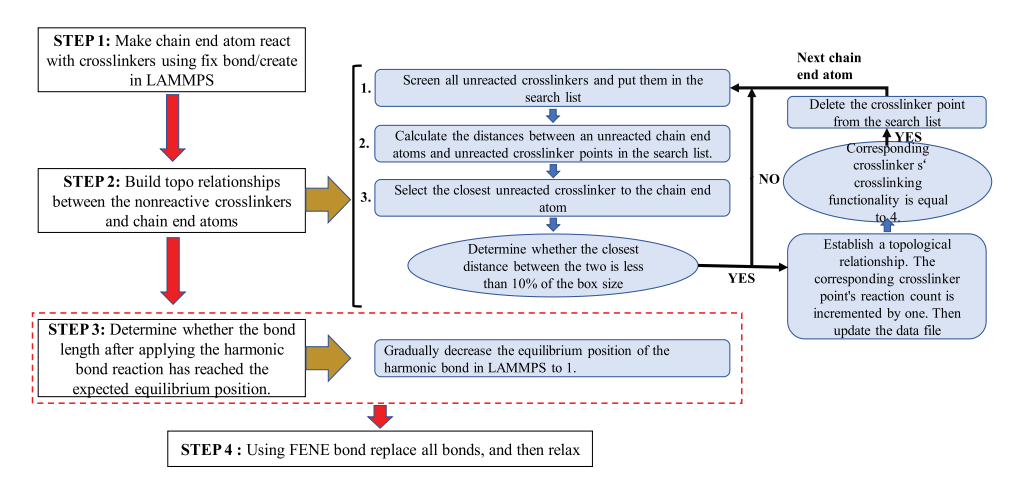


Figure 2. The flowchart showing processes to create highly cross-linked networks for long polymer chain with aid of a soft harmonic bond.

$$E(r) = U_{WCA} + K(r - R_{c,Q})^{2}(r - R_{c,Q} - B_{1})(r - R_{c,Q} - B_{2}) + U_{0}$$
(4)

The bond breakage and the overall mechanical properties of the polymer networks are highly dependent on the parameters of the quartic potential. A comparison of the quartic potentials based on different parameters is illustrated in Figure 1(b). Our choice of the parameters ensures a medium strength of the quartic potential. In the case of recommended values by LAMMPS (K = 1200,  $R_{c,Q} = 1.3$ ,  $B_1 = -0.55$ ,  $B_2 = 0.25$ ,  $U_0 = 34.6878$ ), the bond breakage happens too easily suggesting that the strength is too weak, while the strength is too strong with the parameters proposed by Stevens (K = 1434.3,  $R_{c,O} = 1.5$ ,  $B_1$ =-0.7589,  $B_2$  = 0, $U_0$  = 62.2234) [49]. The scenarios were confirmed by the results of the simulations deforming the N = 20 network with the two sets of the parameters. As shown in Figure S4, when the potential parameter values recommended by Stevens are used, the polymer chain becomes very robust, and the polymer system does not break completely even when the system strain reaches 15. However, when using the potential parameter values recommended in LAMMPS, the system shows drastic fluctuations, and the entire system breaks completely shortly after the stretching begins. Therefore, to prevent the polymer system from being too strong or too fragile, we have fitted a new set of potential parameter values (K = 1434.3,  $R_{c,Q} = 1.5$ ,  $B_1 = -0.72$ ,  $B_2 = -0.23$ ,  $U_0 = 41$ ) in this paper, which are located between the potential parameter values recommended by Stevens and LAMMPS, as shown in Figure 1(b). The detailed fitting process is described below. As given in Equation 4, the energy required for a bond breaking is closely related to the parameters of K,  $R_{c,Q}$ ,  $B_1$ ,  $B_2$  and  $U_0$ .  $R_{c,Q}$  is the cutoff distance for quartic bond and it is set equal to 1.5, the same as the stretch limit of the FENE bond. The value K = 1434.3 is adopted from Stevens [49]. The overall height of the energy landscape is dependent predominantly on  $U_0$ , as shown in Figure S5 (a). The value of  $U_0 = 41.0$  is fixed to ensure that the energy landscape lies between the setting of Stevens parameter values and LAMMPS recommended parameter values. At the end, the values of  $B_1$  and  $B_2$  are tuned to ensure the energy minima is within 2% deviation from the setting of Stevens parameter values.

#### 2.3. Deformation

Uniaxial deformation was applied to the networks to determine their mechanical properties. The stretching rate used in this paper is  $1 \times 10^{-3}$ . During the uniaxial tension process, a system was subjected stretch along the z direction with an assigned engineering strain rate, while the simulation box was shrunk along the other two directions accordingly. It is important to highlight that macroscopic fractures in the networks are typically depicted by a damage process where cracks propagate through mesoscopic tips, leading to the creation of voids and volume changes. However, the scale (both in terms of length and time) covered by the MD simulation is much more limited compared to the macroscopic damage process. As a result, the microcanonical (NVT) ensemble was employed to ensure the incompressibility of the networks, allowing us to concentrate on their structural evolution, such as bond breakages and alterations in the primitive path. The Irving-Kirkwood formula was used to calculate the stress components and the stresses were monitored during the tension process [50]. The nominal stress  $\sigma_N$  is defined by Eq. 5, calculated by the stress components in all three directions.

$$\sigma \equiv \sigma_{zz} - \frac{1}{2} \left( \sigma_{xx} + \sigma_{yy} \right) \tag{5}$$

#### 2.4. Entanglement analysis

The Z1+ algorithm was used to obtain the entanglement information of the network [36]. The algorithm conducts geometric optimization to identify the primitive path of the entangled chains. In the optimization, all the ends of all polymer chains are frozen in space. The contours of the chains are then shrunk simultaneously into zigzag segments that resemble the original chain configuration, but without violating the uncrossability from the other chains, such as the average number of kinks,  $\langle Z \rangle$ . Thus,  $\langle Z \rangle$  formed by the zigzag segments can be defined and used to quantify numbers of entanglement. The tube diameter, a quantification of the constraining strength of the entanglement, is defined as  $a_{\rm pp} = \langle R_{\rm ee}^2 \rangle / \langle L_{\rm pp} \rangle$  where  $\langle R_{\rm ee}^2 \rangle$  and  $\langle L_{\rm pp} \rangle$  are the mean-squared end-to-end distance and mean contour length of the identified primitive paths, respectively. Accordingly, the degree of polymerization for an entanglement,  $\langle N_{\rm e} \rangle$  can be defined.

#### 3. Results and discussion

Polymers can be classified as unentangled polymers and entangled polymers based on the presence or absence of entanglement [51]. In this study, our primary focus is understanding the factors influencing the mechanical properties of both unentangled and entangled polymers during various stretching stages. In Section 3.1, we delve into the role of the crosslinking network on the tensile behavior of unentangled polymers. Drawing from insights in Section 3.1, we then weaken the crosslinking bonds in Section 3.2. This helps us determine the extent to which the strength of these bonds influences the overall tensile properties, thereby deepening our grasp on their role during stretching. Subsequently, we analyze how the interplay of entanglements, and the crosslinking network affects the tensile characteristics of entangled polymer systems. In section

3.4, we quantitatively present the roles of entanglement and the crosslinking network during the stretching process. Here, we extract specific parameters to better understand the impacts of both entanglements and the crosslinking network. The stress-strain curve is particularly illuminating, showcasing the relationship between the material's stress (force per unit area) and strain (deformation). The number of broken bonds ( $n_B$ ) provides a side perspective on the integrity of the polymer system during stretching. The normalized end-to-end distance ( $\langle R_{ee} \rangle$ ) helps to characterize the straightening status of the polymer chain during stretching, especially changes in the slope of the curve which indicate the resistance the polymer-chain encounters during the straightening process. Typically, for a linear unentangled polymer chain, the changes in the slope of the normalized  $\langle R_{ee} \rangle$  are minimal when its transitions from a completely relaxed state to a fully straightened state [52]. This is due to the polymer chain experiencing uniform resistance during this process. The changes in the bond length of all bonds within system  $(I_b)$ distribution can help to provides insight into the force distribution of all bonds within the polymer at various tensile moment, while the evolution of the mean bond length of all bonds within system  $(\bar{l}_h)$  with the extensive strain can help to compare the force acting on the bonds at the different moments of the stretching process.

#### 3.1. Stretching of unentangled polymer networks

Results in Figure 3 quantify the structural evolution of N=20 network from the onset of extension to complete fracture ( $\sigma=0$ ) under two distinct potential function value combinations. The parameter changes shown in Figure 3 (a-f) offer key insights into the system's

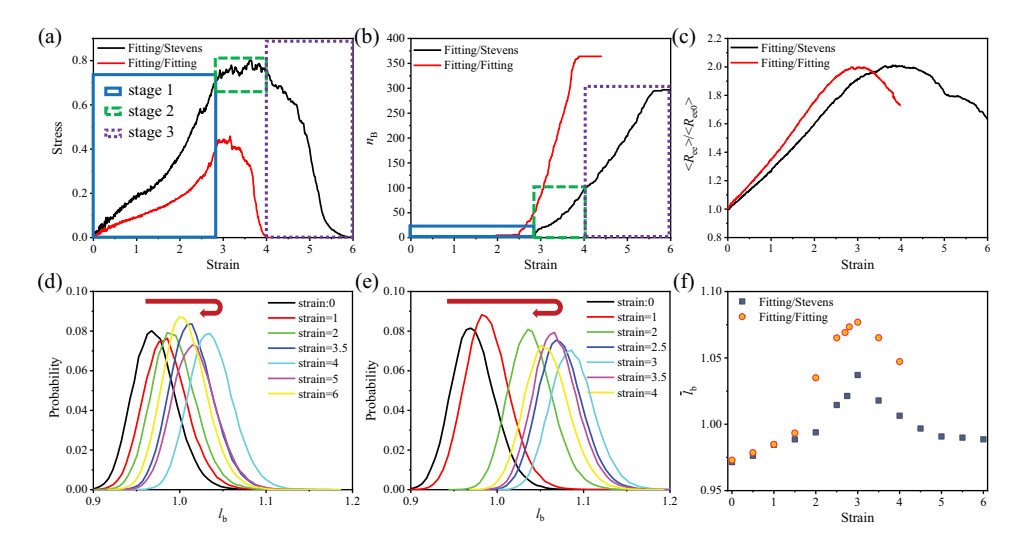


Figure 3. The stretch of unentangled network (N20) with different potential parameters value setting for crosslinkers: (a) stress–strain curves for the stretched system with N=20 and different potential function value settings for crosslinking bonds, (b) the change of the number of broken bonds ( $n_B$ ) with the strain, (c) normalized end-to-end distance  $< R_{\rm ee} > vs.$  strain, (d) the bond length ( $I_b$ ) distribution (all bonds) with the change of strain for the potential setting Fitting/Stevens, (e) the bond length ( $I_b$ ) distribution (all bonds) with the change of strain for the potential setting Fitting/Fitting, and (f) the change of mean bond length ( $I_b$ ) with strain.

evolution during stretching, enhancing our comprehension of the crosslinking network's role in the stretching of unentangled crosslinked polymers. From Figure 3, the potential setting combination Fitting/Fitting and the potential setting combination Fitting/Stevens show similar tendency but different values, we first use the potential setting combination of Fitting/Stevens (the black line in Figure 3) to show what the role of crosslinking network has played during the process of stretching for unentangled polymer systems.

Figure 3(a) displays the stress response of the crosslinked polymer through three clear stages as strain increases. Initially, from a strain of roughly 0 to 3, the stress rises almost linearly with strain. In the second stage, between strains of around 3 and 4, the stress remains relatively constant, even as the strain continues to increase. After this point, as the strain rises further, the stress begins to decline. As observed in Figure 3(b), almost no bonds break in the first stage, suggesting that the polymer network retains its integrity despite the deformation during this phase. However, when the deformation enters the second, the value of  $n_{\rm B}$  increases nearly linearly with the further stretching. Considering the uniform stretching of the polymer network throughout, the slope of the curve in this plot signifies the bond-breaking rate. This suggests that when deformation enters the second stage, the  $n_{\rm B}$  value in the unentangled polymer network decreases uniformly.

Figure 3(c) illustrates the changes in the normalized  $\langle R_{ee} \rangle$  with strain throughout the entire stretching process. During the first stage, the  $\langle R_{ee} \rangle$  of the polymer chains increases nearly linearly with the increase in deformation, suggesting that the chains follow affine deformation. As deformation progresses into the second stage, the increase in the polymer chain's  $\langle R_{ee} \rangle$  begins to decelerate. The changes in  $n_B$  and in  $\langle R_{ee} \rangle$ show that in this stage, parts of the chains are highly stretched to the limit suggested by the Langevin chain model. Chains in the highly stretched state are prone to breakage, if not already broken. But the network maintained its integrity in this stage because the number of broken chains is limited. When considering the material's uniform stretching, it becomes evident that the polymer chains, behaving as Langevin chains, face heightened resistance during stretching compared to the initial stage. This aligns with observations from Figure 3(b), where bond breakage commences. This implies that some of the primary load-bearing bonds have reached their load limit and start to fracture. Yet, since few bonds break, the stress can maintain a relatively high level even with increased deformation. This limited change in stress, despite the strain, accounts for the near-stable stressstrain curve observed in the second stage of Figure 3(a). In the third stage, the value of  $< R_{\rm ee} >$  decrease after reaching a peak shown in the second stage because of the accumulated damage done to the network in the previous stage such that the loadbearing capacity of the network decrease.

As the bonds break, as shown on Figure 3(b), segments of chains are liberated from the bulk network. Since they are free, they tend to relax from the high-energy and stretched state back to the equilibrium state. Figure 3(d) depicts the distribution of  $I_b$  during the stretching process. The mean of the distribution shifts rightward as deformation increases but shifts leftward afterward because of the network's damage. The change of the mean bond length,  $\bar{I}_b$ , of all bonds within the system is shown in Figure 3(f). The increase of  $\bar{I}_b$  corresponds to the first and the second stage of the deformation, while the decrease represents the third stage.



#### 3.2. The change of the strength of the crosslinking bond

Many studies underscore the influence of the crosslinking density on the mechanical properties of the crosslinked system. It is widely accepted that, within specific bounds, amplifying the crosslinking density can increase the network's modulus [53,54]. The Influence of the crosslinking bond's strength on the tensile properties of the network is detailed in this section.

For a given polymer system with a constant crosslinking density, it is possible to form various types of crosslinking bonds between polymer chains. These bonds can be either covalent or ionic and can be formed either during the polymerization process or postpolymerization [55–57]. Typically, covalent bonds are stronger than ionic bonds. As a result, different crosslinking bond types can lead to networks with diverse mechanical properties, like overall strength and resilience. As the quartic potential function values fitted in this study are weaker than the potential function values used in the research of Stevens [49], we set the crosslinking bonds to be the potential function values used by Stevens and those fitted in this study, respectively, and compare their effect of the tensile process.

Figure 3(a) illustrates that by decreasing the strength of the crosslinking bond, there is a pronounced drop in the material's peak stress, and the strain at which complete fracture occurs is significantly reduced. When comparing the evolutions in  $\langle R_{ee} \rangle$  in Figure 3(c), it is noticed that the network with stronger crosslinking bonds is less stretched than the network with weaker counterpart at the same applied strain. This infers that an increase in the strength of crosslinking bonds correspondingly enhances the strength of the network. The changes of the distribution  $l_{\rm b}$  under two sets of potential values are shown in Figures 3(d,e). The changes in  $\bar{l}_b$  are shown in Figure 3(f). While the evolutions of  $ar{l}_{
m b}$  share similar trend, the peak values are significantly different showing that the weaker crosslinking bond indeed make the network easier to stretch. In addition, our analysis of the bond breakage location revealed that when potential function values proposed by Stevens are used for the crosslinking bond, all bond breaking occur at the chain's internal bond. In contrast, when we use the potential function values we derived in this study for the crosslinking bond, about 10% of bond breakages occur at the crosslinking sites. Therefore, the analyses on strain-induced alterations in the networks, presented hereafter, are all with the combination of the Fitting/Stevens potential function values for the polymer chains and crosslinking bonds.

#### 3.3. Stretch of entangled polymer networks

In sections 3.1 and 3.2, we investigated the role of crosslinking during the stretching of unentangled polymers. From this section onwards, we shift our focus to understanding the roles that both the crosslinking and entanglement play in the stretching process, using a polymer system with a chain length of N = 1000 as a case study. The stress–strain curve of the entangled system resembles the result of the unentangled case, although the second stage is notably short. For a precise definition of the second stage, it is determined that the polymer deformation enters this stage when the stress reaches 90% of the maximum stress. As shown in Figure 4(a), during the first stage, the stress increases linearly with strain. Upon entering the second stage, the fluctuation in stress

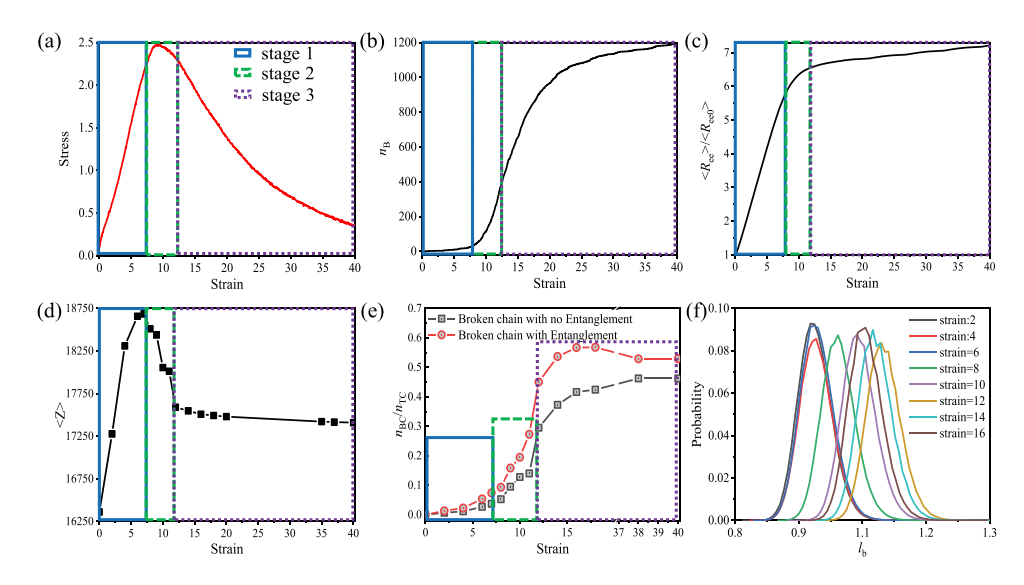


Figure 4. The stretch of entangled crosslinking polymer systems (N1000) using the potential setting of Fitting/Stevens for the chain's inner bonds and crosslinking bonds respectively: (a) stress–strain curves for the stretched system, (b) the change of the number of broken bonds ( $n_B$ ) with the strain, (c) normalized end-to-end distance  $R_{\rm ee}$  vs. strain, (d) the number of entanglements with the change of strain, (e) the ratio of number of broken chains ( $n_{\rm BC}$ ) to total chains ( $n_{\rm TC}$ ), which includes the ratio of broken chain with entanglement and the ratio of broken with no entanglement, and (f) the change of bond length distribution with strain.

values is minimal (maximum: 10%). As deformation progresses into the third stage, the stress response significantly reduces with increasing strain, though complete fracture (i.e. stress value reaching zero) is not observed within the simulated stretching range. The change of broken number of bonds  $n_B$  in Figure 4(b) illustrates the network's integrity throughout the stretching process. During the first stage of deformation, only a negligible number of bonds break as strain increases, indicating that the network integrity is largely preserved during this stage. Upon transitioning into the second stage, a significant increase in  $n_{\rm B}$  is noted as strain progresses. Unlike in the unentangled system, the slope of the curve during this stage steadily escalates, reflecting a gradual increase in the rate of bond breakage. At the junction of the second and third stages, n<sub>B</sub> almost linearly increases with strain. As the third stage approaches its end, the rate of bond breakage begins to taper off, resulting in a progressive flattening of the curve. Figure 4(c) presents the changes in normalized  $\langle R_{ee} \rangle$  as a function of the strain. The value of  $\langle R_{ee} \rangle$  incrementally rises with strain, ultimately tending toward a constant value. On transitioning into the second stage, the curve's slope progressively steepens, suggesting the polymer chains enter the highly stretch state during this phase. This is further evidenced by the shifting in  $I_{\rm b}$  distribution with strain (Figure 4(f)). From this figure, it is clear that during the first stage,  $I_{\rm b}$  remains relatively stable despite the strain increase, implying the bonds within the system are either forceless or subjected to negligible force. As the deformation enters the second stage, a discernible rightward shift in  $I_b$  distribution is observed, reflecting that more bonds start to be subjected to force in the second stage. This may account for the progressive decrease in the  $< R_{ee} >$  's slope during this stage. Upon entering the third

stage, the  $< R_{\rm ee} >$  value stabilizes with strain increase. This differs from the previously studied unentangled polymer. This is primarily due to the negative correlation between entropic spring stiffness and polymer-chain length. As chain length increases, this value decreases, and the polymer chain scarcely retracts. Thus, as a substantial number of bonds break,  $\langle R_{ee} \rangle$  gradually reaches a constant value. The  $I_b$  also decreases in this stage. The tendency for the change of  $I_b$  occurring in the entangled polymer system is like the N20 system. As shown in Figure 4(e), the integrity of the network has been destroyed severely in the third stage. Some chains therefore have no force acting on, which causes the decreasing of the  $I_h$ .

Figure 4(d) depicts the change in the number of entanglements ( $\langle Z \rangle$ ) throughout the stretching process. In the initial stage, the  $\langle Z \rangle$  value rises notably with increasing strain. This is primarily because as the length of the simulation box along the stretch direction increases, the cross-sectional area of the simulation box contracts, resulting in closer proximity between polymer chains and an increase in their aggregation degree. This is corroborated by the local configuration changes in the polymer network from Figure 5(c, d). Furthermore, as illustrated by the red dashed line in Figure 5(d2), as some chains straighten during this process, their contact surface area with other chains grows. These two factors likely lead to an increase in system entanglements during this phase. As the system moves into the second stage, there is a marked reduction in the number of entanglements. This is because more bonds are subject to force during this process, and the polymer chain is gradually straightened, see Figure 5(e). From Figure 4(e), it is evident that during the first stage, nearly no chains break, and the fraction of broken chains in the system devoid of entanglements is also low. Hence, throughout this phase, entanglements maintain a minimal level. However, as the strain increases and the deformation enters the second stage, the percentage of broken chains without entanglements

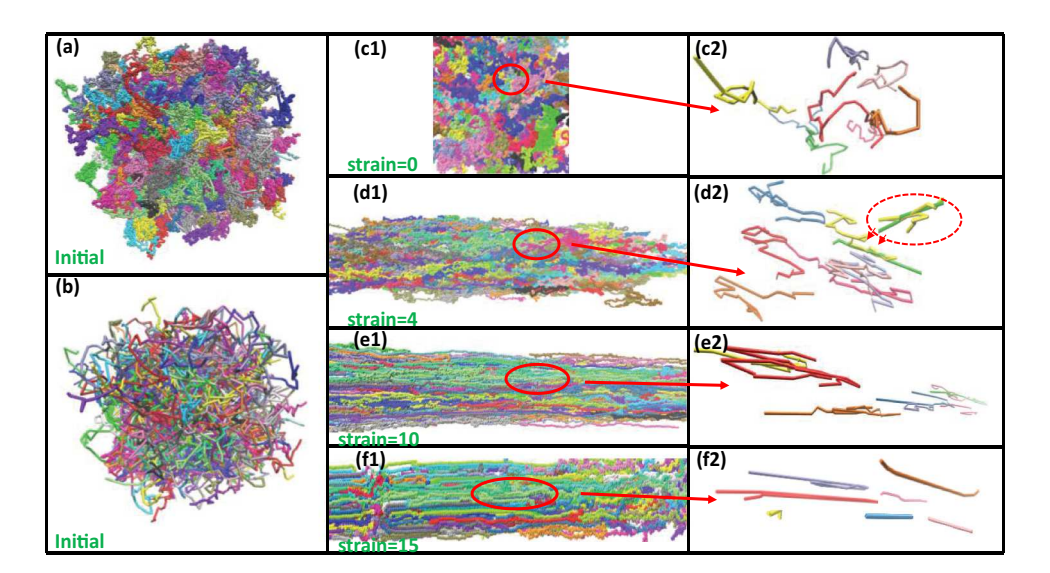


Figure 5. The evolution of polymer's configuration during the stretching process: (a) snapshot of initial polymer chains, (b) initial primitive paths (PPs), (c1) and (c2) the polymer chains configuration (left) and initial primitive paths (right) at the strain equal to 0, (d1) and (d2) strain=4, (e1) and (e2) strain=10, and (f1) and (f2) strain=15.

grows, resulting in a notable decrease in the system's overall entanglements. Upon reaching the third stage, the number of entanglements in the system slowly decreases because a considerable number of chains break. Significantly, there is a marked increase in the number of segments without entanglements as the deformation transits from the second to the third stage. This leads to a pronounced decline in the number of entanglements in this phase. As the strain increases in the third stage, the growth of chains lacking entanglements slows down, likely accounting for the tapering decrease in the system's overall entanglement count. Such dynamics can also be visualized from Figure 5(f). In this stage, numerous chains break down into shorter chains, which significantly curtails the system's entanglement count.

The combined analysis sheds light on the roles of entanglement and crosslinking throughout the entangled polymer network's stretching. In the initial stage, as highlighted in Figure 4(b), minimal bonds break, implying that the polymer network maintains a high level of integrity. Simultaneously, the number of entanglements markedly rises (see Figure 4(e)). However, no significant shifts occur in the material's bond length suggesting that the elasticity of the network is still an entropic effect and that entanglement plays a pivotal role during this stage. Being the primary load-bearing mechanism, entanglements first absorb the external load placed on the network during the initial stage, and determines the peak stress of the network. In the second stage, the number of entanglements within the system dramatically drops, while the value of  $n_{\rm B}$  increases, indicating that the internal bonds of the system begin to react to external forces. The subsequent rightward shift in the bond length distribution highlights an elongation of these bonds. While some bonds start to fracture, their numbers remain limited, ensuring that the polymer network largely maintains its integrity.

Consequently, integrating the present analysis offers the understanding that as the deformation continues to increase, certain entanglements surpass their load-bearing threshold and begin to slip. This leads to the straightening of the polymer chain observed in Figure 5(e1). At this state, the load-bearing element within the system starts to transit toward the polymer bonds. As the  $n_B$  continues to increase, the polymer network's integrity is significantly compromised, leading the system's transition into the third phase. This elucidates that our observation in the second stage, as represented in Figure 4(b), that a gradual incline in the curve's slope. In the initial part of the second stage, the entanglements primarily absorb the applied stress, preventing the network bonds from experiencing direct external pressures. As a result, bond breakage occurs at a reduced pace. However, as strain increases and a significant number of entanglements decrease, more bonds directly bear the load, leading to a faster rate of bond breakage. In summary, the increase in entanglement quantity is the key factor keeping the entangled polymer system in the first stage. The reduction in entanglement numbers instigates the transition from the first to the second phase, while the network sustains the system within the second phase. Ultimately, the network's disintegration triggers the system's transition into the third stage. The research findings presented in this paper regarding the role of entanglements in crosslinked polymers validate the hypotheses put forth by Suo et al. [15]. In their work, they designed a polymer wherein the entanglement count notably surpasses that of cross-link, resulting in a pronounced enhancement in the network's mechanical properties. They hypothesized that this might be because, during the stretching process, the entanglements enable the transfer of tensile forces acting on a polymer

chain to other chains, leading to a more uniform force distribution within the system. This finding aligns with the observations in our study, where the entanglements serve a load-bearing role in the initial stage of stretching.

Although the case N1000 shows the roles of the entanglement in the stretching process, the number of entanglements per chain in this system remains relatively modest (around 20 entanglements per chain). To validate these conclusions in highly entangled polymers, we have extracted data from a longer chain length of 8408 (227 entanglements per chain) in the entangled polymer and studied the variations of relevant parameters during the stretching process, as shown in Figure S6, where it can be observed that the information reflected is generally consistent with the information provided in Figure 4. Therefore, we believe that the conclusions drawn from the above analysis are generally applicable to highly entangled polymers.

#### 3.4. The correlation of entanglement and crosslinking with tensile stress

The results shown in section 3.3 the roles of entanglement during the network tensile process, highlighting its strong interplay with tensile stress. To delve deeper into this connection, we normalized the alterations in the number of entanglements  $\Delta \langle Z \rangle$ , as well as the  $n_B$  at the three stages, against the tensile stress ( $\sigma$ ). These are visualized in Figure 6. Figure 6(a) demonstrates the correlation between the normalized augmentation in entanglement throughout the first stage of stretching and the maximum tensile stress in this stage ( $\sigma_{\text{max,S1}}$ ). We observe a positive linear relationship between the growth in entanglement and fluctuations in tensile stress. This observation is further corroborated by Figure 6(c), which indicates that the normalized number of broken chains ( $n_{BC}$ ) remains constant with increasing stress during the first stage. This underpins our prior conclusion

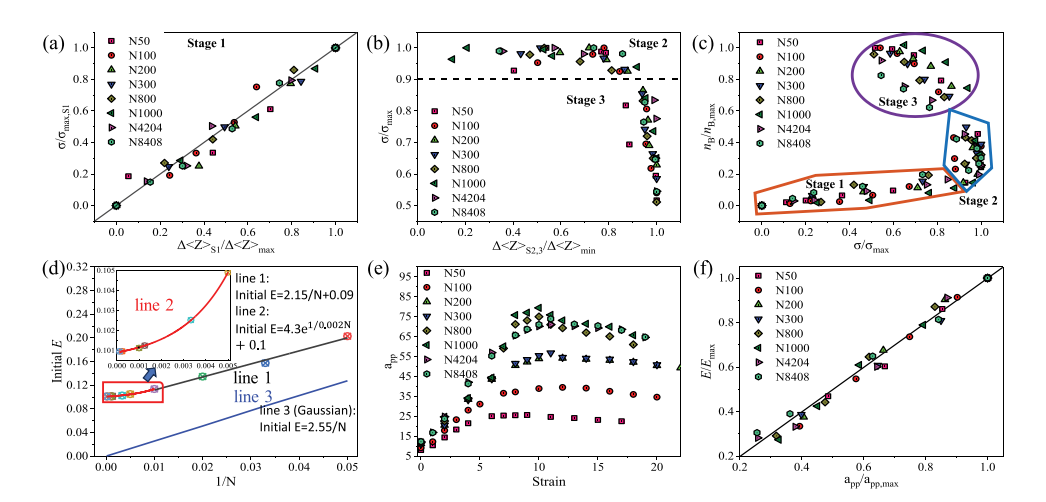


**Figure 6.** The correlation between the entanglement as well as crosslinking network and the tensile stress: (a) the normalized change of entanglements number with the normalized tensile stress in stage 1, (b) the normalized change of entanglements number with the normalized tensile stress in stage 2 and stage 3, (c) the normalized tensile stress vs. normalized number of broken chains  $(n_{bc})$ , (d) the initial elastic modulus (E) changes with the reciprocal of the chain length, (e) the change of tube diameter with the strain and (f) the normalized elastic modulus vs. normalized tube diameter.

that entanglements operate as primary load-bearers in the first stage, and the quantity of entanglement within the system establishes the tensile stress of the entangled crosslinking polymer during the elastic phase. Figure 6(b) illustrates the relationship between the normalized entanglement decrease during the second and third stretching stages and the maximum tensile stress in these stages. Considering this encompasses the second stage, the maximum tensile stress during this phase also signifies the material's highest tensile stress over the entire stretching process. In Figure 6(c), it is shown that during the second stage, despite the decreasing number of entanglements and disruption of the network, stress value does not change much. From the discussions in Section 3.3, it is evident that the combined effects of reduced entanglements and the retained integrity of the crosslinking network leads to the emergence of the second stage. Therefore, it is not surprising that their respective correlations with tensile stress in the second stage are low. In the third stage, it is observed that the correlation between the normalized quantity of entanglements within the system and tensile stress is low, with no significant alteration accompanying an increase in tensile stress. However, there exists a negative correlation between the normalized  $n_B$  and tensile stress, lending further confirmation of the finding in Section 3.3, suggesting that the damage of the crosslinking network contributes to a decline in tensile stress within the system during the third stage.

The microstructure of the entangled network has been analyzed. To quantify the macroscopic elastic property of the network, the Young's modulus, *E*, is estimated from the slope of the stress–strain curves in Figures 3(a) and 4(a). The modulus *E* is defined by averaging the slopes up to 0.1 of strain.

We first explore the relationship between initial E with the chain length, as shown in Figure 6(d) and the relationship between E with the tube diameter  $a_{pp}$ , as shown in Figure 6(f). In Figure 6(d), it is shown that the value of E displays a linear decline as the chain length changes from unentangled to entangled regime (from N20 to N100). The value remains stable once it enters the highly entangled regime, as there is almost no significant change in the initial E value when the chain length is over 1000. Longer polymer chains tend to have more conformational possibilities and greater flexibility [58]. When subjected to stress, these chains can uncoil and extend to accommodate the applied force, leading to a reduced E value because of their ability to deform more before breaking. In addition, longer chains can result in more entanglement of the polymer chains. This increased entanglement can lead to a decreased response to stress because the chains are less able to align in the direction of the stress [59]. We also have compared the estimated E value with the counterpart predicted by the Gaussian and the tube models. The comparison is shown in Figure 6(d). The modulus predicted by the Gaussian model is calculated according to the shear modulus  $G_x = \rho_c k_B T$ , where  $\rho_c$  is the number density of the chains. On the other hand, the entanglement modulus,  $G_e =$ 0.0128, has been given in the work of Svaneborg et al. [47]. With the assumption of incompressibility, i.e. Poisson's ratio v = 0.5, the corresponding Young's moduli are calculated according to  $E_x = 2G_x(1 + \nu)$  and  $E_e = 2G_e(1 + \nu)$  it is worth noting that the moduli estimated from our MD simulations are higher than the theoretical predictions because of the enthalpic (bond stretching) effect of the dynamic loading in the MD simulation. On the other hand, the Gaussian and the tube model only consider the entropic effect. The enthalpic effect is suggested by the change in the bond length, which is related to the

elongation and breakage of the quartic bonds. We have examined the change in the system's tube diameter in response to strain as shown in Figure 6(e). The result reveals that for a constant polymer system, as the stretch length increases, the  $a_{\rm pp}$  value shows a trend of increasing first and then tending toward a constant value, where the increase in the  $a_{\rm pp}$  value occurs in the first stage. In addition, we have also extracted the change in  $a_{\rm pp}$  value with different chain lengths of the polymer system and found that as the chain length of the polymer system increases, the  $a_{\rm pp}$  value shows a trend of first increasing and then remaining unchanged, such as when the chain length increases to over 800, its  $a_{\rm pp}$  value remains consistent in spite of the increase in chain length. Finally, the relationship between  $a_{\rm pp}$  and E in the first stage is shown in Figure 6(f), which shows a strong correlation between  $a_{\rm pp}$  value and E value. Based on the analysis above, it is concluded that the chain length determines the initial E value, and the E increase with stretching.

The analysis and research results have shown how the crosslinking networks with and without entanglements present different tensile properties. In unentangled polymers, this research underscores the profound impact of crosslinking bond strength on the polymer system's overall strength and resistance to deformation. The findings provide new thoughts for materials design to improve the tensile strength of the unentangled polymer systems. For entangled polymers, a notable discovery is the pivotal role of entanglement in load-bearing during the elastic stages of stretching. As stretching continues and entanglement decreases, the responsibility of load-bearing transfers to the network bonds. This provides direction for the design of highly stretchable polymers and more resilient materials. Overall, these findings highlight the interplay between entanglement and crosslinking in the stretching processes of highly entangled polymer networks. Such insights pave the way for advanced design strategies in polymeric materials, targeting specific mechanical properties.

#### 4. Conclusions

In conclusion, this research sheds light on the pivotal roles that entanglement and the crosslinking network play during the stretching of entangled polymer systems. The comprehensive analysis demonstrates that the intricate interplay between the crosslinking bond strength, entanglement, and their influence on the polymer system's tensile stress. First, we analyze the stretching process of unentangled polymer system and show that the strength of the crosslinking bond is an important factor affecting the overall strength of the networks. A reduction in the strength of the crosslinking bond substantially elevates the rate of bond breakage, decreasing the network's load-bearing capacity. Then, in examining the stretching process of the entangled polymer system, it is shown that in the early phase of stretching, the entanglements serve as the primary load-bearing mechanism and determine the maximum stress the entangled network can endure during elastic deformation. As the stretching process progresses, we note a reduction in the number of entanglements, shifting the load-bearing role onto the individual bonds. This shifting is crucial for the transition of the system from the first to the second stage. Subsequently, the continued stretching process leads to the destruction of the polymer network, marking the system's transition into the third stage which is characterized by an

accelerated rate of bond breakage, resulting in a severe disruption to the network's integrity and a decrease in the system's tensile strength. Furthermore, through normalization, we have further confirmed the connections between the shifts in entanglement number, the breakdown of the crosslinking network, and the tensile stress within the entangled system. The increase in entanglement corresponds to the increase in tensile stress in the first stage, which exists a linear correlation between them, while the destruction of the network correlates with the decrease in tensile stress during the third stage. In summary, our research provides an understanding of the complex interplay between the entanglement and the elasticity of the network.

#### Disclosure statement

No potential conflict of interest was reported by the author(s).

#### **Funding**

Y.L. gratefully acknowledges financial support from the U.S. National Science Foundation (CMMI-2314424, CMMI-2316200, and CAREER Award CMMI-2323108) and 3 M's Non-Tenured Faculty Award. Support for this research was also provided by the University of Wisconsin-Madison, Office of the Vice Chancellor for Research and Graduate Education with funding from the Wisconsin Alumni Research Foundation.

#### **Author statement**

Yuhao Liu: methodology, software, validation, formal analysis, data curation, Writing - original draft, visualization. Weikang Xian: methodology, software, formal analysis, data curation, writing – original draft, writing - review & editing, Visualization. Jinlong He: validation, methodology, software, writing - review & editing. Ying Li: conceptualization, methodology, software, writing - review & editing, supervision, project administration, funding acquisition.

#### Data and code availability

The data that support the findings of this work are available from the corresponding author upon reasonable request. All noncommercial numerical codes to reproduce the findings of this study are available from the corresponding author upon reasonable request.

#### References

- [1] Treloar L. Elastic recovery and plastic flow in raw rubber. Rubber Chem Technol. 1940;13 (4):795-806. doi: 10.5254/1.3546559
- [2] Edwards SF. Statistical mechanics with topological constraints: I. Proc Phys Soc Lond. 1967;91 (3):513. doi: 10.1088/0370-1328/91/3/301
- [3] Warner M, Edwards SF. Neutron scattering from strained polymer networks. J Phys A Math Gen. 1978;11(8):1649–1655. doi: 10.1088/0305-4470/11/8/024
- [4] Rubinstein M, Panyukov S. Nonaffine deformation and elasticity of polymer networks. Macromolecules. 1997;30(25):8036–8044. doi: 10.1021/ma970364k
- [5] Rubinstein M, Panyukov S. Elasticity of polymer networks. Macromolecules. 2002;35 (17):6670-6686. doi: 10.1021/ma0203849



- [6] Kaliske M, Heinrich G. An extended tube-model for rubber elasticity: statistical-mechanical theory and finite element implementation. Rubber Chem Technol. 1999;72(4):602–632. doi: 10.5254/1.3538822
- [7] Mergell B, Everaers R. Tube models for rubber–Elastic systems. Macromolecules. 2001;34 (16):5675–5686. doi: 10.1021/ma002228c
- [8] Davidson JD, Goulbourne NC. A nonaffine network model for elastomers undergoing finite deformations. J Mech Phys Solids. 2013;61(8):1784–1797. doi: 10.1016/j.jmps.2013.03.009
- [9] Xiang YH, Zhong DM, Wang P, et al. A general constitutive model of soft elastomers. J Mech Phys Solids. 2018;117:110–122. doi: 10.1016/j.jmps.2018.04.016
- [10] Degennes PG. Reptation of a polymer chain in the presence of fixed obstacles. J Chem Phys. 1971;55(2):572–579. doi: 10.1063/1.1675789
- [11] Doi M, Edwards SF. Dynamics of concentrated polymer systems .1. Brownian motion in the equilibrium state. J Chem Soc Faraday Trans. 1978;74:1789–1801. doi: 10.1039/F29787401789
- [12] Berry GC, Fox TG. The viscosity of polymers and their concentrated solutions. In: Fortschritte der Hochpolymeren-Forschung. Springer; 2006. pp. 261–357. doi:10.1007/BFb0050985.
- [13] Yamamoto T, Campbell JA, Panyukov S, et al. Scaling theory of swelling and deswelling of polymer networks. Macromolecules. 2022;55(9):3588–3601. doi: 10.1021/acs.macromol. 1c02553
- [14] Urayama K, Kohjiya S. Extensive stretch of polysiloxane network chains with random- and super-coiled conformations. Eur Phys J B. 1998;2(1):75–78. doi: 10.1007/s100510050227
- [15] Kim J, Zhang GG, Shi MX, et al. Fracture, fatigue, and friction of polymers in which entanglements greatly outnumber cross-links. Science. 2021;374(6564):212–216. doi: 10.1126/science. abg6320
- [16] Liu PY, Zhang Y, Guan Y, et al. Peptide-crosslinked, highly entangled hydrogels with excellent mechanical properties but ultra-low solid content. Adv Mater. 2023;35(13):9. doi: 10.1002/ adma.202210021
- [17] Fu L, Li L, Bian Q, et al. Cartilage-like protein hydrogels engineered via entanglement. Nature. 2023;618(7966):740–747. doi: 10.1038/s41586-023-06037-0
- [18] Huang T, Xu HG, Jiao KX, et al. A novel hydrogel with high mechanical strength: a macromolecular microsphere composite hydrogel. Adv Mater. 2007;19(12):1622–1626. doi: 10.1002/adma.200602533
- [19] Kessel B, Lee M, Bonato A, et al. 3D bioprinting of macroporous materials based on entangled hydrogel microstrands. Adv Sci. 2020;7(18):13. doi: 10.1002/advs.202001419
- [20] Lake GJ, Thomas AG. The strength of highly elastic materials. Proc Math Phys Eng Sci. 1967;300:108. doi:10.1098/rspa.1967.0160
- [21] Zheng DC, Lin ST, Ni JH, et al. Fracture and fatigue of entangled and unentangled polymer networks. Extreme Mech Lett. 2022;51:10. doi: 10.1016/j.eml.2022.101608
- [22] Long R, Hui CY, Gong JP, et al. The fracture of highly deformable soft materials: a tale of two length scales. Annu Rev Condens Matter Phys. 2021;12(1):71–94. doi: 10.1146/annurev-conmatphys-042020-023937
- [23] Khiem VN, Mai TT, Urayama K, et al. A multiaxial theory of double network hydrogels. Macromolecules. 2019;52(15):5937–5947. doi: 10.1021/acs.macromol.9b01044
- [24] Lamont SC, Weishaar K, Bruns CJ, et al. Micromechanics and damage in slide-ring networks. Phys Rev E. 2023;107(4):13. doi: 10.1103/PhysRevE.107.044501
- [25] Li Y, Abberton BC, Kroger M, et al. Challenges in multiscale modeling of polymer dynamics. Polymers. 2013;5(2):751–832. doi: 10.3390/polym5020751
- [26] Matsuda T, Kawakami R, Nakajima T, et al. Revisiting the origins of the fracture energy of tough double-network hydrogels with quantitative mechanochemical characterization of the damage zone. Macromolecules. 2021;54(22):10331–10339. doi: 10.1021/acs.macromol. 1c01214
- [27] Zhou YC, Schroeder CM. Dynamically heterogeneous relaxation of entangled polymer chains. Phys Rev Lett. 2018;120(26):6. doi: 10.1103/PhysRevLett.120.267801
- [28] Ferry JD. Viscoelastic properties of polymers. New York: John Wiley & Sons; 1980.



- [29] McLeish TCB. Tube theory of entangled polymer dynamics. Adv Phys. 2002;51(6):1379–1527. doi: 10.1080/00018730210153216
- [30] Kremer F, Schönhals A. Broadband dielectric spectroscopy. Springer Science & Business Media: 2002. doi: 10.1007/978-3-642-56120-7
- [31] Everaers R, Sukumaran SK, Grest GS, et al. Rheology and microscopic topology of entangled polymeric liquids. Science. 2004;303(5659):823-826. doi: 10.1126/science.1091215
- [32] Stephanou PS, Baig C, Tsolou G, et al. Quantifying chain reptation in entangled polymer melts: topological and dynamical mapping of atomistic simulation results onto the tube model. J Chem Phys. 2010;132(12):16. doi: 10.1063/1.3361674
- [33] Likhtman AE, Ponmurugan M. Microscopic definition of polymer entanglements. Macromolecules. 2014;47(4):1470-1481. doi: 10.1021/ma4022532
- [34] Tzoumanekas C, Theodorou DN. Topological analysis of linear polymer melts: a statistical approach. Macromolecules. 2006;39(13):4592-4604. doi: 10.1021/ma0607057
- [35] Shanbhag S, Kroger M. Primitive path networks generated by annealing and geometrical methods: insights into differences. Macromolecules. 2007;40(8):2897-2903. doi: 10.1021/ ma062457k
- [36] Kroger M, Dietz JD, Hoy RS, et al. The Z1+package: shortest multiple disconnected path for the analysis of entanglements in macromolecular systems. Comput Phys Commun. 2023;283:13. doi: 10.1016/j.cpc.2022.108567
- [37] Li Y, Tang S, Abberton BC, et al. A predictive multiscale computational framework for viscoelastic properties of linear polymers. Polymer. 2012;53(25):5935-5952. doi: 10.1016/j. polymer.2012.09.055
- [38] Sliozberg YR, Hoy RS, Mrozek RA, et al. Role of entanglements and bond scission in high strain-rate deformation of polymer gels. Polymer. 2014;55(10):2543-2551. doi: 10.1016/j. polymer.2014.03.051
- [39] Umeno Y, Kubo A, Albina JM. Coarse-grained molecular dynamics simulation of deformation and fracture in polycarbonate: effect of molar mass and entanglement, theor. Appl Fract Mech. 2020;109:7. doi: 10.1016/j.tafmec.2020.102699
- [40] Higuchi Y, Saito K, Sakai T, et al. Fracture process of double-network gels by coarse-grained molecular dynamics simulation. Macromolecules. 2018;51(8):3075-3087. doi: 10.1021/acs. macromol.8b00124
- [41] Kremer K, Grest GS. Dynamics of entangled linear polymer melts: a molecular-dynamics simulation. J Chem Phys. 1990;92(8):5057-5086. doi: 10.1063/1.458541
- [42] Faller R, Kolb A, Muller-Plathe F. Local chain ordering in amorphous polymer melts: influence of chain stiffness. Phys Chem Chem Phys. 1999;1(9):2071-2076. doi: 10.1039/a809796h
- [43] FrantzDale B, Plimpton SJ, Shephard MS. Software components for parallel multiscale simulation: an example with LAMMPS, Eng. Comput. 2010;26(2):205-211. doi: 10.1007/s00366-009-0156-z
- [44] Auhl R, Everaers R, Grest GS, et al. Equilibration of long chain polymer melts in computer simulations. J Chem Phys. 2003;119(24):12718–12728. doi: 10.1063/1.1628670
- [45] Sides SW, Grest GS, Stevens MJ, et al. Effect of end-tethered polymers on surface adhesion of glassy polymers. J Polym Sci Pt B-Polym Phys. 2004;42(2):199–208. doi: 10.1002/polb.10672
- [46] Svaneborg C, Everaers R. Multiscale equilibration of highly entangled isotropic model polymer melts. J Chem Phys. 2023;158(5):21. doi: 10.1063/5.0123431
- [47] Gula IA, Karimi-Varzaneh HA, Svaneborg C. Computational study of cross-link and entanglement contributions to the elastic properties of model PDMS networks. Macromolecules. 2020;53(16):6907-6927. doi: 10.1021/acs.macromol.0c00682
- [48] Sorichetti V, Ninarello A, Ruiz-Franco JM, et al. Effect of chain polydispersity on the elasticity of disordered polymer networks. Macromolecules. 2021;54(8):3769-3779. doi: 10.1021/acs. macromol.1c00176
- [49] Stevens MJ. Interfacial fracture between highly cross-linked polymer networks and a solid surface: effect of interfacial bond density. Macromolecules. 2001;34(8):2710-2718. doi: 10. 1021/ma000553u



- [50] Irving JH, Kirkwood JG. The statistical mechanical theory of transport processes .4. The equations of hydrodynamics. J Chem Phys. 1950;18(6):817–829. doi: 10.1063/1.1747782
- [51] Masubuchi Y. Contraction of entangled polymers after large step shear deformations in slip-link simulations. Polymers. 2019;11(2):9. doi: 10.3390/polym11020370
- [52] Wohlfarth K, Woehler C. Wavelength-dependent seeing systematically changes the normalized slope of telescopic reflectance spectra of mercury. Remote Sens. 2022;14(2):18. doi: 10. 3390/rs14020405
- [53] Ren YQ, Sun XJ, Chen LL, et al. Structures and impact strength variation of chemically crosslinked high-density polyethylene: effect of crosslinking density. RSC Adv. 2021;11 (12):6791–6797. doi: 10.1039/D0RA10365A
- [54] Bornstein D, Pazur RJ. The sulfur reversion process in natural rubber in terms of crosslink density and crosslink density distribution. Polym Test. 2020;88:10. doi: 10.1016/j.polymertest ing.2020.106524
- [55] Zhu Q, Barney CW, Erk KA. Effect of ionic crosslinking on the swelling and mechanical response of model superabsorbent polymer hydrogels for internally cured concrete, Mater. Mater Struct. 2015;48(7):2261–2276. doi: 10.1617/s11527-014-0308-5
- [56] Shokuhfar A, Arab B. The effect of cross linking density on the mechanical properties and structure of the epoxy polymers: molecular dynamics simulation. J Mol Model. 2013;19 (9):3719–3731. doi: 10.1007/s00894-013-1906-9
- [57] Scheutz GM, Elgoyhen J, Bentz KC, et al. Mediating covalent crosslinking of single-chain nanoparticles through solvophobicity in organic solvents. Polym Chem. 2021;12 (31):4462–4466. doi: 10.1039/D1PY00780G
- [58] Jiang ZT, Dou WH, Sun TT, et al. Effects of chain flexibility on the conformational behavior of a single polymer chain. J Polym Res. 2015;22(12):9. doi: 10.1007/s10965-015-0875-3
- [59] Namsheer K, Rout CS. Conducting polymers: a comprehensive review on recent advances in synthesis, properties and applications. RSC Adv. 2021;11(10):5659–5697. doi: 10.1039/ D0RA07800J